Planar Hall effect and uniaxial in-plane magnetic anisotropy in Mn δ-doped GaAs/*p*-AlGaAs heterostructures

A. M. Nazmul,[1] H. T. Lin,[2] S. N. Tran,[1] S. Ohya,[1,3] and M. Tanaka[1,3]
[1]*Department of Electronic Engineering, The University of Tokyo, 7-3-1 Hongo, Bunkyoku, Tokyo 113-8656, Japan*
[2]*Department of Materials Science and Engineering, National Tsing-Hua University, Hsinchu 300, Taiwan, Republic of China*
[3]*Japan Science and Technology Agency, 4-1-8 Honcho, Kawaguchi, Saitama 332-0012, Japan*
(Received 1 June 2006; published 2 April 2008)

We have studied the planar Hall effect (PHE) in a Mn δ-doped GaAs-based heterostructure consisting of Mn δ-doped GaAs and *p*-type AlGaAs. We observe a distinct and large PHE and a specific in-plane [110] uniaxial magnetic anisotropy below the ferromagnetic transition temperature (T_C). This uniaxial in-plane magnetic anisotropy is found dominant over the biaxial cubic anisotropy, and is clearly identified by the angular dependence of PHE. This observation is quantitatively discussed in terms of two models of magnetization reversal: the coherent rotation model and the domain-wall motion model. The model calculation fit to the experimental data makes it possible to determine the uniaxial and cubic anisotropy fields and examine the behavior of magnetization reversal.

DOI: 10.1103/PhysRevB.77.155203 PACS number(s): 71.55.Eq, 75.50.Pp, 72.20.My, 72.25.Dc

I. INTRODUCTION

Much attention has been paid over the past decade to the carrier-induced ferromagnetism in III-V based magnetic alloy semiconductors (MASs) such as (In,Mn) (Refs. 1 and 2) and (Ga,Mn)As,[3,4] which may lead to applications to a new class of spintronic devices. However, since the ferromagnetic transition temperature (T_C) is still far below room temperature, device application remains to be a challenge. Theoretical calculations predict that the T_C values are determined by the Mn concentration and hole density, which are both limited in III-V based MAS, and the highest T_C reported so far are 90 K in (InMn)As,[5] 173 K in (GaMn)As,[6] and 130 K in (InGaMn)As.[7] Very recently, it has been reported that the Mn δ-doped GaAs/*p*-type AlGaAs heterostructures show significant enhancement of ferromagnetic transition temperature T_C.[8–10] In the heterostructures, Mn δ-doping approach allows locally high Mn concentration, and holes were supplied from the *p*-type Be-doped AlGaAs layer to the Mn δ-doped GaAs layer. Therefore, the interaction between the magnetic dopants (Mn) and two-dimensional hole gas leads to ferromagnetic ordering with relatively high T_C of 172–250 K.[9,10]

From the viewpoint of both fundamental research and applications, magnetic anisotropy plays a vital role for various purposes. It was recently revealed that (Ga,Mn)As epilayers have a cubic magnetic anisotropy with the easy axis of ⟨100⟩ at low temperature[11–16] and showed a change to the uniaxial anisotropy with the easy axis of [110] with increasing temperature.[17,18] To characterize the magnetic properties of ultrathin films and heterostructures on which bulk magnetization measurements are difficult, Hall effect measurements are very powerful and, thus, often used for the study of MAS thin film materials.

In this paper, we study the *planar* Hall effect (PHE) and magnetic anisotropy of a Mn δ-doped GaAs/*p*-AlGaAs heterostructure, which have not been studied so far. We observed large PHE in the heterostructure, which allows examination of the in-plane magnetization and other important magnetic characters, such as T_C, magnetic anisotropy, and magnetization switching process. In particular, the magnetic anisotropy is characterized by the angular dependence of PHE and quantitatively discussed in terms of two models of magnetization reversal: (1) the coherent rotation model and (2) the domain-wall motion model. Our comparative analysis between the model calculations and the experimental results makes it possible to determine the uniaxial and cubic anisotropy fields and examine the behavior of magnetization reversal.

II. PLANAR HALL EFFECT

The Hall effect can provide extensive information about magnetic properties of materials. When a current is applied through a ferromagnetic thin film, as illustrated in Fig. 1(a), the resulting Hall voltage V_{xy} can be expressed as follows:[19–21]

$$V_{xy} = \frac{R_0 I}{t} B \cos \alpha + \frac{\mu_0 R_S I}{t} M_\perp + \frac{kI}{t} M_\parallel^2 \sin 2\varphi. \quad (1)$$

Here, I is the applied current, $B(=\mu_0 H)$ is the external magnetic field flux density, $M_\perp$ and $M_\parallel$ are the perpendicular and in-plane components of magnetization M, and t is the film thickness, respectively. R_0, R_S, and k are the ordinary Hall coefficient, the anomalous Hall coefficient, and a constant related to the anisotropic magnetoresistance effect, respectively. α and θ_H are the angle of the external field direction with respect to the perpendicular (z) axis and the angle of the in-plane projected field vector (in the x-y plane) with respect to the current direction, respectively. φ is the angle between the in-plane magnetization ($M_\parallel$) direction and applied current (I). The first, second, and third terms in Eq. (1) express the ordinary Hall effect, anomalous Hall effect (AHE), and PHE, respectively. In particular, the dominant contribution from AHE and PHE in ferromagnetic alloy semiconductors makes it possible to determine the magnetic properties of the perpendicular component and the in-plane component, respectively. Hence, when B is applied along the film plane ($\alpha = 90°$), Eq. (1) can be simplified as

 ©2008 The American Physical Society

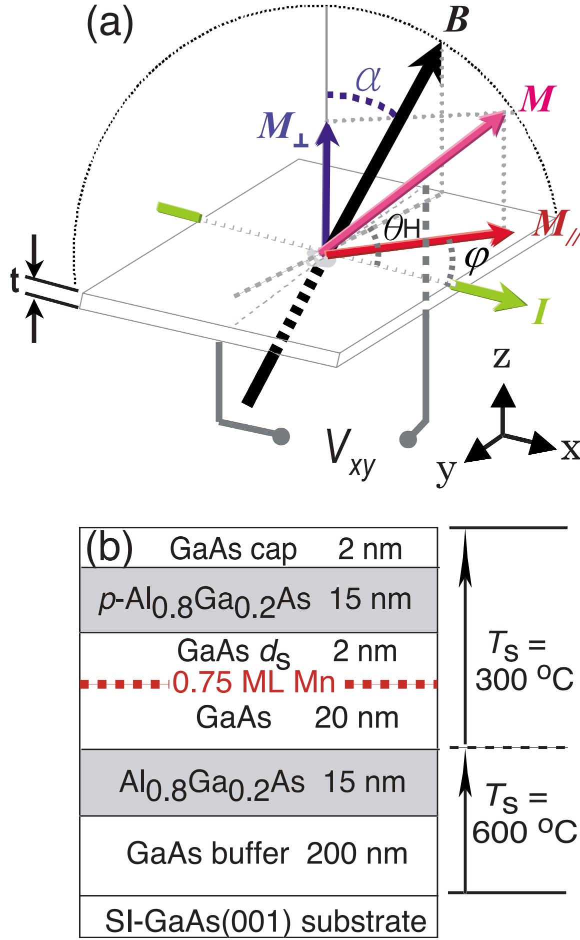

FIG. 1. (Color online) (a) Schematic diagram of the general Hall effect experiments. For the PHE measurements, the external magnetic field $B(=\mu_0 H)$ is applied in-plane ($\alpha=90°$). (b) Sample structure studied in this paper, which is a *p*-type heterostructure with Mn δ-doping grown by MBE on a SI GaAs (001) substrate. The Mn coverage in δ-doped layer is 0.75 ML. The undoped separation layer thickness d_S is 2 nm.

$$V_{xy} = \frac{kI}{t} M_{\parallel}^2 \sin 2\varphi. \tag{2}$$

The planar Hall effect voltage given by Eq. (2) is proportional to the square of in-plane magnetization $M_{\parallel}$ and $\sin 2\varphi$, which are determined by the intensity and direction of the external magnetic field. Based on the PHE data, it is, thus, possible to monitor the magnetization direction and draw conclusions on the magnetic anisotropy of the material. In this study, we focus on the PHE measurements in order to examine the in-plane magnetization and magnetic anisotropy of a Mn δ-doped GaAs/*p*-AlGaAs heterostructure. For this purpose, we have set the external magnetic field (H) parallel to the film plane, thus the angle α is set to 90°. The experimental data are discussed in terms of two models of magnetization reversal: (1) the coherent rotation model and (2) the domain-wall motion model. Details of the model calculations in Mn δ-doped GaAs heterostructures will be described in Sec. V.

III. MOLECULAR BEAM EPITAXY GROWTH AND EXPERIMENTAL DETAILS

A *p*-type modulation-doped heterostructure with Mn δ-doping, whose structure is shown in Fig. 1(b), was grown by molecular beam epitaxy (MBE) on a semi-insulating (SI) GaAs (001) substrate. First, we grew a 200 nm undoped GaAs buffer layer and a 15-nm-thick undoped $Al_{0.8}Ga_{0.2}As$ layer at 600 °C. Then, the substrate temperature was cooled down to 300 °C, and we grew a 20-nm-thick undoped GaAs layer, a 0.75 monolayer (ML) Mn δ-doped layer, a 2-nm-thick undoped GaAs separation layer (d_S), a 15-nm-thick Be-doped $Al_{0.8}Ga_{0.2}As$ layer with a Be concentration of 1.8×10^{18} cm^{-3}, and a thin (5 nm) undoped GaAs cap layer at 300 °C. *In situ* reflection high energy electron diffraction showed a clear streaky pattern of the zinc-blende-type structure throughout the growth, and (1×2) reconstruction was observed during and after the growth of the Mn δ-doped layer. In the heterostructure, holes are supplied from the overgrown *p*-AlGaAs layer to the Mn δ-doped GaAs layer (d_S=2 nm), resembling a normal high-electron-mobility transistor.

Magnetotransport measurements were carried out in three Hall bars with 50 μm width and 200 μm length, fabricated by conventional photolithography and wet chemical etching. The long axis (current direction) of the Hall bars was aligned along the three principal crystalline orientations [110], $[\bar{1}10]$, and [100] in order to examine the magnetic anisotropy of the heterostructure. The dc current (I=50 μA) was supplied along the long axis of the Hall bars (x axis), and the transverse voltage V_{xy} (y axis) was measured to obtain the Hall resistance (R_{xy}), as illustrated in Fig. 1(a). For angular dependence measurements, samples were mounted on a rotating stage so that we can vary the angle (θ_H) between the current (I) and the applied magnetic field (H). The electrical contacts were made using gold wire leads and indium solder to form Ohmic contacts. The samples were set in a cryostat with an AlGaAs diode temperature sensor, and the temperature was varied from 2.6 to 300 K.

IV. TEMPERATURE DEPENDENCE OF THE PLANAR HALL EFFECT

First, we measured the temperature dependence of the planar Hall resistance R_{xy} (V_{xy}/I) of the heterostructure of Fig. 1(b), when the current (I) direction was aligned along $[\bar{1}10]$, and the angle (θ_H) between the current and external in-plane magnetic field was fixed at 10°. The applied magnetic field (H) was slowly swept from 1000 to −1000 G and, finally, back to 1000 G. Unlike the odd function signals of AHE, the PHE shows even function signals with respect to the magnetic field, as shown in Fig. 2(a). Two resistance jumps were clearly observed in the sweeps, and the negative- and positive-field sweeps are even symmetric within the applied field for temperature below 55 K. The magnitude of both PHE resistance jumps (ΔR_{PH}) and the switching field (H_{sw}) decreased rapidly with increasing temperature. Here, as illustrated in Fig. 2(a), H_{sw} is defined by the magnetic field at which negative- and positive-field sweeps meet,[15] and

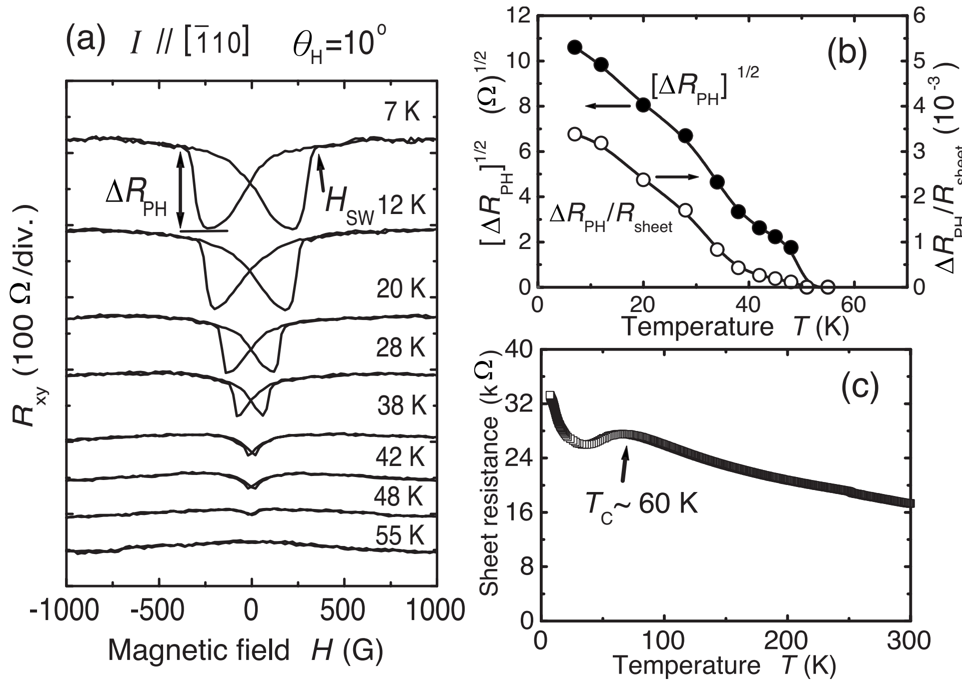

FIG. 2. (a) Magnetic field dependence of the planar Hall resistance (R_{xy}) at various temperatures from 7 to 55 K. The current I direction was set along $[\bar{1}10]$, and applied field H orientation was in plane ($\alpha=90°$) and fixed at $\theta_H=+10°$. (b) Temperature dependence of $\Delta R_{PH}/R_{sheet}$ (open circles) and $\sqrt{\Delta R_{PH}}$ (closed circles) derived from (a). (c) Temperature dependence of the sheet resistance R_{sheet} of the Mn δ-doped GaAs heterostructure.

ΔR_{PH} is defined by the Hall resistance (R_{xy}) difference between the lowest point and H_{sw} point.[11]

The ferromagnetic transition temperature (T_C) of the heterostructure was determined from the temperature (T) dependence of $\Delta R_{PH}/R_{sheet}$ and $\sqrt{\Delta R_{PH}}$ derived from Fig. 2(a) for $T<60$ K, as shown by open and closed circles in Fig. 2(b). Here, R_{sheet} is the zero-field sheet resistance. Note that $\Delta R_{PH}/R_{sheet}$ and $\sqrt{\Delta R_{PH}}$ are proportional to the hole spin polarization[11] and in-plane magnetization $M_{\parallel}$,[21,22] respectively. On the other hand, temperature dependence of sheet resistance (R_{sheet}-T) and AHE was measured. The R_{sheet}-T curve in Fig. 2(c) shows a local maximum hump around 60 K due to the critical scattering, suggesting that T_C is ~60 K. This value of T_C was also confirmed by the Curie-Weiss fitting from the temperature dependence of AHE in the paramagnetic state at $T>60$ K, indicating that the T_C value is ~57 K, which is in good agreement with the disappearance of the PHE jumps (~55 K) and the local maximum in the R_{sheet}-T trace (~60 K). These results indicate that PHE is a suitable tool for characterizing the magnetic properties of ultrathin films and heterostructures.

V. ANGULAR DEPENDENCE OF PLANAR HALL EFFECT AND MAGNETIC ANISOTROPY

A. Magnetic field and angular dependence of planar Hall effect

We studied the magnetic field dependence and the angular (θ_H) dependence of PHE. The estimated misalignment of the angles is around ±5° when we mount the samples on the rotating stage of the measurement system. Figure 3(a) shows the field dependence of PHE (open circles in R_{xy}-H data) when the field orientation angle θ_H was varied from −90° to 45°. The current direction was set along $[\bar{1}10]$ and the temperature was fixed at 2.6 K. The solid lines in the plots are model calculation fits to the experimental data, as will be described later. Three important features are clearly observed in Fig. 3(a). The first is large switching events: at distinct magnetic fields (H_{sw}), two jumps were observed in $R_{xy}(H)$. This behavior resembles the behavior of the giant planar Hall effect in (Ga,Mn)As epilayers.[11,23] The magnitude of Hall jumps in the present Mn δ-doped GaAs/p-AlGaAs heterostructure is as large as 300 Ω. Previously reported values are ~80–100 Ω (Refs. 11 and 23) for GaMnAs and ~130 Ω (Ref. 24) for LaSrMnO. The second important feature is the specific angular dependence behavior of $R_{xy}(H)$; the sign of the Hall jump (ΔR_{PH}) suddenly changed from positive to negative at around $\theta_H=0°$. The H_{sw} and the ΔR_{PH} slowly decrease when θ_H is away from 0°. Third, in the entire range of the angular dependence, the Hall jumps at the low field areas are not as abrupt as expected from the magnetization reversal model of coherent rotation. The calculation fit by the domain-wall motion model, considering the unpinning of the domain wall at the low field areas, can well reproduce the experimental data with suitable fitting parameters (as will be discussed later).

The magnetization reversal process can be deduced from the above results in the following way. For the case of $\theta_H=+45°$, the reversal process can be described by the sequence A→B→C→D in Fig. 3(a) when the field sweep was from +1.5 to −1.5 kG, and the corresponding schematic magnetization switching process is illustrated in Fig. 3(b). When the magnetic field (H) was first applied along the [010] direction, at high fields the magnetization (M) was aligned close to the external magnetic field direction, as shown by the A state. Then, when H is close to zero, the magnetization direction is basically aligned along the [110] direction, since the uniaxial anisotropy along the [100] direction is dominant at 2.6 K. When the applied magnetic field gradually swept to a critical field (H_{sw}~270 G), the magnetization direction was suddenly switched from the B state to

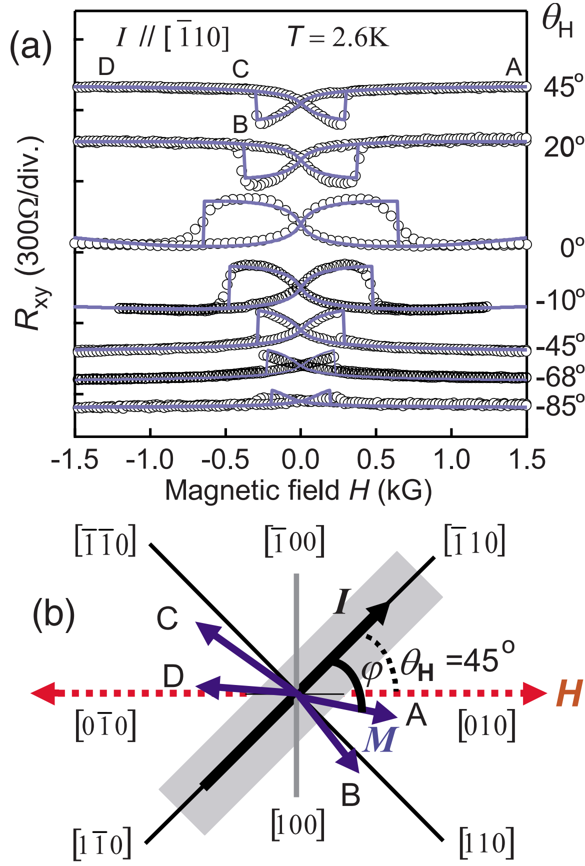

FIG. 3. (Color online) (a) Open circles show the planar Hall resistance (R_{xy}) for various field orientations θ_H from $-85°$ to $+45°$ measured at 2.6 K. The solid lines in the plots are model calculation fits to the experimental data for H_{KU}=840 G, H_{KC}=640 G, and E_{pin}/M=370 G. (b) Schematic diagram of the magnetization reversal process for θ_H=+45° in the film plane of the sample.

the more stable C state. Finally, with increasing negative field, M was gradually aligned close to the field direction, as illustrated by the D state.

B. Modeling of the results and anisotropy fields

To account for the measured PHE resistance behavior as a function of applied magnetic field, we first begin with the Stoner-Wohlfarth formulation of coherent rotation reversal of magnetization, where the total energy E of an arbitrary single domain magnetization orientation is[11,12,18]

$$E = K_U \cos^2 \varphi + \frac{K_C}{4} \cos^2 2\varphi - MH \cos(\varphi - \theta_H). \quad (3)$$

Here, K_U and K_C are the in-plane uniaxial and cubic magnetic anisotropy constants, M is the magnetization, H is the applied field, and φ and θ_H are the directions of M and H with respect to the [$\bar{1}$10] direction [schematically defined in Figs. 1(a) and 3(b)]. For the Stoner-Wohlfarth formulation for coherent rotation reversals, the resulting magnetization orientation φ for a given applied field takes the value that satisfies a local minimum in $E(\varphi)$. For a fixed orientation θ_H and intensity of the applied field H, the equilibrium magnetization state can be described as $\partial E/\partial\varphi=0$ and $\partial^2 E/\partial^2\varphi >0$. Here, two fitting parameters, the uniaxial anisotropy field $H_{KU}=2K_U/M$ and the cubic anisotropy field $H_{KC}=2K_C/M$, are introduced to perform model calculations. To obtain H_{KU} and field H_{KC}, $\partial E/\partial\varphi=0$ of Eq. (3) is fed into Eq. (2) after being solved with trial anisotropy fields, and the procedure is iterated to produce the best fit to the data. Figure 4(a) shows the angular dependence of the PHE (R_{xy}) data (open circles) and the calculated fit (solid curve) at a high magnetic field of 5 kG. These fits show good agreement with the experimental results at high fields within an angular variation of $\pm5°$, which occurs from the misalignment of the sample after mounting on the rotating stage. The full-field calculated sweep for θ_H=45° and θ_H=−45° using the derived magnetic anisotropy field parameters (H_{KU}=840 and H_{KC}=640 G) is presented in Fig. 4(b) by dotted lines. This result indicates that the magnetic anisotropy is primarily uniaxial with the easy axis along [110]. However, the Hall resistance jumps occur at lower fields than those obtained by the coherent rotation model fitting.

To account for the real situation in the low field area, we now depart from the Stoner-Wohlfarth formulation by allowing the magnetization orientation to change from one local minimum state to another via a domain structure change through the sweeping of domain walls. In this model, we take a phenomenological constant E_{pin} as the pinning energy at the defect energy barriers which the domain wall encounters as it propagates, as schematically shown in Fig. 4(c). We fit this parameter in the switching positions (H_{sw}) by assuming that if the single domain energy of Eq. (3) exceeds E_{pin}, it will transit to a new energy minimum, which means that the magnetization orientation changes. In an attempt to estimate this energy, the fitting parameter E_{pin}/M is combined with the coherent rotation model in such a way that the H_{sw} in the low field area are fitted well. In this manner, the estimated E_{pin}/M value at 2.6 K is 370 G, while H_{KU}=840 and H_{KC}=640 G, derived from the coherent rotation model at high fields, are kept unaltered. These values produce the solid lines in Figs. 4(b) and 3(a). The two jumps throughout the entire angular range of the experimental data agree well with this result. Figure 5 shows the domain-wall model calculation fits to the measured data of two other Hall bars with current orientations along the [110] and [100] directions. Here, clear $R_{xy}(H)$ switching behaviors were also observed in both of the current directions. We found that the estimated H_{KU} and H_{KC} values at 2.6 K globally fitted well with these two current orientations within a dispersion of ±60 G and ±40 G, respectively. The dispersion of the E_{pin}/M value was large (±100 G), probably due to the inhomogeneities among the Hall bars.

Pursuing the above model analysis based on the dominant uniaxial axis along the [110] direction, one finds that the H_{sw} at which these switching events take place can be deduced by formulating $E_{[110]}-E_{[\bar{1}\bar{1}0]}=E_{pin}$, where E_{pin} is a 180° domain-wall pinning energy. Then, based on Eq. (3), the H_{sw} for the current direction along the [110] can be expressed as[17,25] $H_{sw}=E_{pin}/2MH|\cos\theta_H|$. Similar procedure for other current directions produced the solid line fits on the angular dependence of switching field data (open circles) in Figs. 6(a)–6(c) with I set along the [$\bar{1}$10], [100], and [110] directions, re-

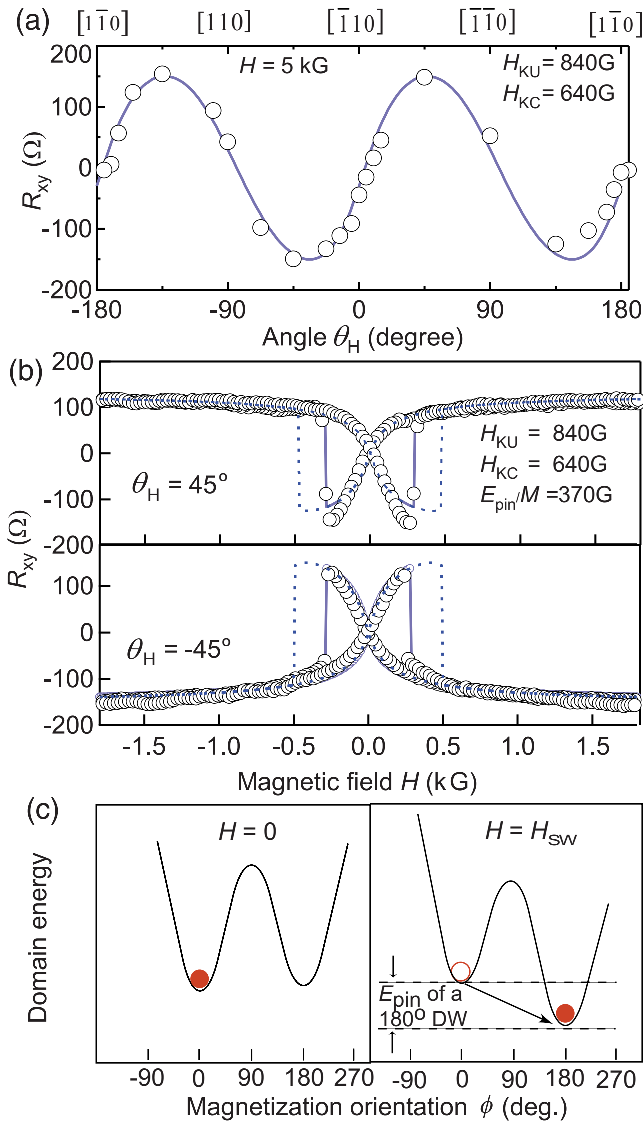

FIG. 4. (Color online) Angular dependence of the planar Hall resistance (R_{xy}-θ_H) at a high magnetic field of H=5 kG at 2.6 K when the current I is along the [$\bar{1}$10] direction. The solid line is the coherent rotation model fit for H_{KU}=840 G and H_{KC}=640 G. (b) Open circles show the R_{xy} data of the heterostructure measured at 2.6 K for two different field orientations, θ_H=45° and θ_H=−45°. The dotted and solid lines are model calculation fits produced without and with E_{pin}/M=370 G, respectively, for H_{KU}=840 G and H_{KC}=640 G. (c) Schematic diagram of a domain-wall motion model showing changes of magnetization orientation through a 180° domain-wall (DW) motion, where E_{pin} is the pinning energy of the DW.

spectively. The E_{pin} value was set to 370 G, derived from the previous domain-wall model fit. The corresponding crystalline orientations are described on the top of each figure. In Fig. 6(a), where I was set along [$\bar{1}$10], two large clear peaks located at 0° and 180° were observed. The symmetric peaks also at [$\bar{1}$10] and [1$\bar{1}$0] directions suggest the presence of an in-plane uniaxial anisotropy along the [110] direction. These two peaks shifted to −45°, 135° and −90°, 90° when I was set along [100] in Fig. 6(b) and along [110] in Fig. 6(c),

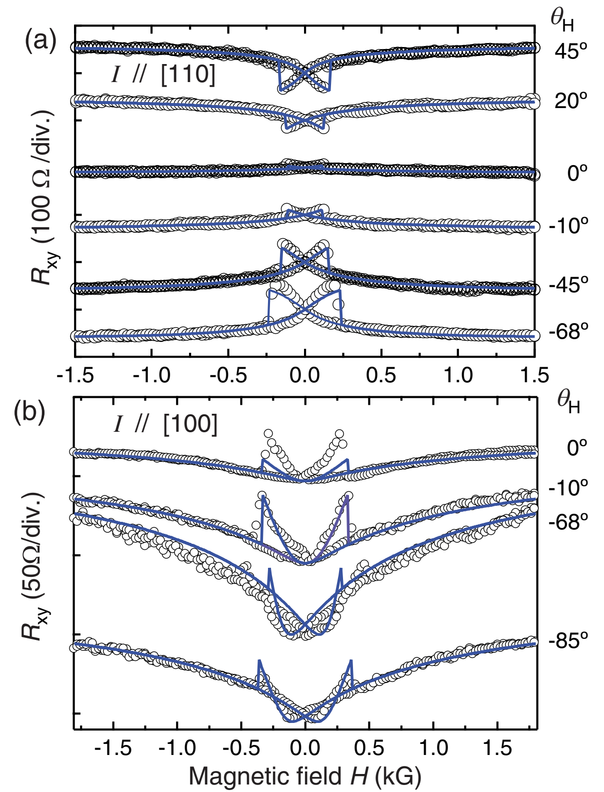

FIG. 5. (Color online) [(a) and (b)] Open circles show the R_{xy} data at 2.6 K for various field orientations θ_H from −85° to +45°, while current directions are along [110] and [100], respectively. The solid lines in the plots are model calculation fits to the experimental data for H_{KU}=840 G, H_{KC}=640 G, and E_{pin}/M=370 G.

respectively. These results clearly indicate that the switching field has no dependence on the orientation of current, and self-consistently confirm the presence of the in-plane uniaxial anisotropy along the [110] direction. These fitting results shown by the solid curves in Figs. 6(a)–6(c) for $E_{pin}/M \approx 370 \pm 100$ G are consistent with the global fittings in the previous figures.

C. Temperature dependence of magnetic anisotropy

The temperature dependence of magnetic anisotropy fields H_{KU} and H_{KC} are plotted in Fig. 7. Here, H_{KU} and H_{KC} values are determined by globally fitting to the experimental results at high magnetic fields, and the deviations in the model fits are represented by error bars. Both H_{KU} and H_{KC} show positive values and $H_{KU} > H_{KC}$ below T_C, suggesting that the easy axis lies in the (001) plane with uniaxial anisotropy along [110] and crystal anisotropy along ⟨100⟩. The magnitude of H_{KU} and H_{KC} decreases with increasing temperature, and H_{KC} falls to zero at lower temperature (~45 K). However, H_{KU} still retains its higher value, and falls to zero at ~55 K near the T_C. This result indicates that the uniaxial magnetic anisotropy along [110] dominates in the whole range of temperature below T_C.

D. Discussion

The magnetic anisotropy of (GaMn)As epitaxial layers has been widely studied by several groups with various

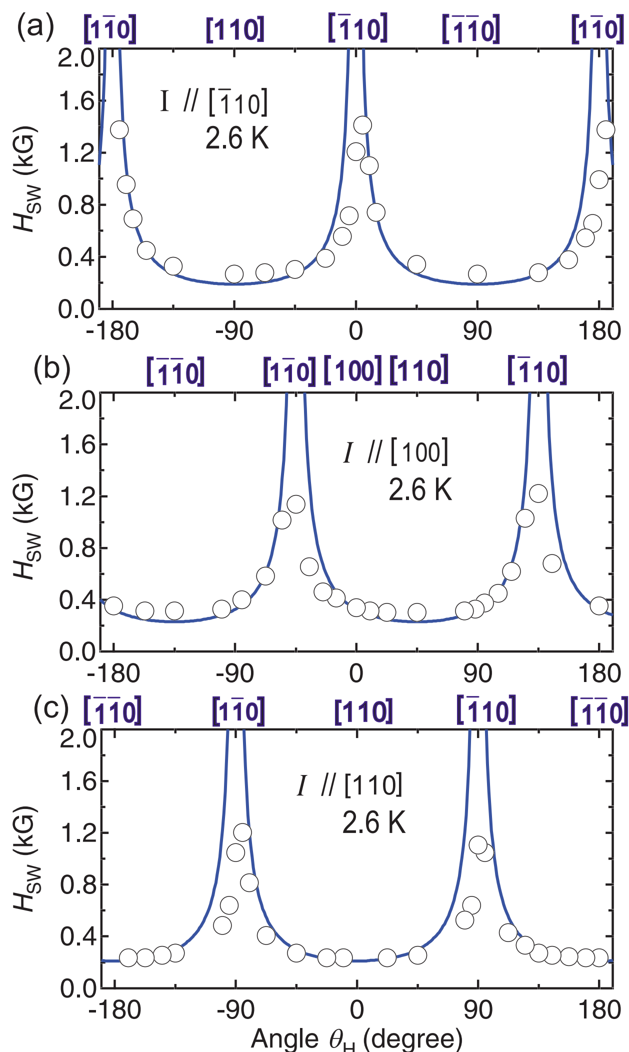

FIG. 6. (Color online) [(a)–(c)] H_{sw} derived from the PHE measurements at 2.6 K as a function of the field orientation (θ_H), where the current directions were set along $[\bar{1}10]$, [110], and [110]. Solid curves are model calculation fits based on the 180° domain-wall motion model (see the text).

methods, e.g., magneto-optical imaging and magnetization measurements,[12,16] ferromagnetic resonance,[26] magnetoresistance,[17] and PHE.[11,15] The occurrence of the uniaxial anisotropy is not expected on the basis of the cubic zinc-blende structure of bulk GaMnAs. The present Mn δ-doped GaAs heterostructure shows the distinct in-plane uniaxial anisotropy field along [110] in the whole temperature range below T_C.

Several theoretical[13,27] and experimental[13–17,25,28] studies showed that the magnetic anisotropy of ferromagnetic semiconductors may be determined by the lattice strain, surface reconstruction, and hole concentration, but the origin of the [110] uniaxial anisotropy is still poorly understood. Based on a strong *p*-*d* exchange coupling between the Mn *d* and the hole's orbitals, Dietl *et al.*[27] predicted that the magnetic properties are closely associated with the symmetry of the valence band, i.e., the magnetic easy axis between ⟨100⟩ and [110] directions for an in-plane magnetized film when all six

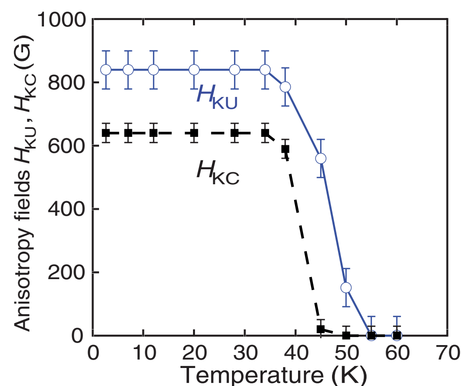

FIG. 7. (Color online) Temperature dependence of the in-plane uniaxial anisotropy field H_{KU} and cubic anisotropy field H_{KC}. Here, H_{KU} and H_{KC} values are determined by globally fitting to the experimental results at high magnetic fields, and the deviations in the model fits are represented by error bars.

subbands at the Γ point involves a band-mixing anisotropic Fermi surface. The present heterostructure of 0.75 ML Mn δ-doped GaAs provides a two-dimensional (2D) density of acceptors equal to $N_{2D} \approx 4.6 \times 10^{14}$ cm^{-2}. Though not straightforward, we can estimate the carrier concentration from the Hall data by excluding the AHE contribution to extract the ordinary Hall effect, and estimate T_c by a Curie-Weiss fitting of the AHE contribution.[9] In this process, the derived sheet hole concentration p_{sheet} is 1.9×10^{13} cm^{-2}. Considering the 2–3 ML (0.58–0.84 nm in width, as observed in transmission electron microscopy study[10]) spatial distribution of the Mn δ-doped layer inside an AlGaAs/GaAs(22 nm)/AlGaAs quantum well, we roughly estimate that three subbands are occupied with holes (self-consistent calculation[29] of a 0.5 ML Mn δ-layer with a 0.5 nm spatial distribution with $p_{sheet} = 1.3 \times 10^{13}$ cm^{-2} showed that holes occupy the first heavy hole, first light hole, and second heavy hole bands). In such a case, it becomes difficult to explain the present [110] uniaxial anisotropy involving a six-band-mixing anisotropic Fermi surface.

It has been shown that epitaxial bcc Fe films grown on (001) GaAs also display uniaxial anisotropy along the [110] direction.[30] It is suggested that this anisotropy is a consequence of the As-dimerization-induced (2×4) and $c(4 \times 4)$ reconstructed surfaces, in which the [110] and the $[\bar{1}10]$ directions are not equivalent, thus causing a uniaxial anisotropy. As described earlier, (1×2) surface reconstruction has been observed during the growth of Mn δ-doped heterostructure, and can cause the uniaxial anisotropy. An additional contribution to the anisotropy can also arise from anisotropic relaxation of strain induced by the lattice mismatch.[31] X-ray analysis indicates that GaMnAs films up to a thickness of 2 μm remain tetragonally strained.[32] Such an anisotropic strain can generate the observed results in our heterostructure.

In a very recent scanning tunneling microscope study,[33] it is shown that when Mn pairs on a GaAs (001) surface is along the [110] direction, the ferromagnetic state is stabilized. This scenario can be related to the strong uniaxial anisotropy observed in the present heterostructure at the entire

range of measurement temperature below the T_C.

The relative strength of the biaxial anisotropy term K_C and uniaxial anisotropy term K_U estimated in the present heterostructure is $K_C:K_U \sim 1:1.3$, and remains almost independent of temperature. In recent reports,[34,35] the anisotropies in bulk GaMnAs have been extensively studied based on the symmetry of the patterns observed in their color coded resistance polar plots of the planar Hall resistance and magnetoresistance. Two uniaxial anisotropies, K_{U1} and K_{U2}, were observed along the $[\bar{1}10]$ and [010] axes together with the biaxial anisotropy K_C along $\langle 100 \rangle$ axes, and relative strengths of the anisotropies at 4 K are of the order of $K_C:K_{U1}:K_{U2} \sim 100:10:1$. The K_{U1} term takes over the biaxial K_C term with increasing temperature, and becomes dominant when temperature is close to the T_C.[35] The contrasting difference between the ratios of anisotropy terms of the two systems may infer a difference in the origin of the anisotropies. However, the origin of the multiple uniaxial anisotropy terms in the bulk system (in this case, two terms) is not clear either.

VI. SUMMARY

We have investigated the PHE of the Mn δ-doped GaAs/p-AlGaAs heterostructure. A large PHE was clearly observed, which makes it possible to examine the in-plane magnetic properties of the heterostructure. The ferromagnetic transition temperature estimated by the temperature dependence of PHE has shown good agreement with the AHE and R_{sheet}-T measurement results. From the characteristics of the angular dependence of PHE, the magnetization reversal behavior has been studied by the model calculations and by fitting to the experimental data. The uniaxial anisotropy field $H_{KU}=840 \pm 60$ G along [110] and the cubic anisotropy field $H_{KC}=640 \pm 40$ G along $\langle 100 \rangle$ were observed at 2.6 K. The in-plane [110] uniaxial magnetic anisotropy was dominant in the whole temperature range below T_C. This indicates that the magnetization reversal process in our heterostructure was strongly influenced by the uniaxial magnetic anisotropy.

ACKNOWLEDGMENTS

This work was partly supported by the Special Coordination Programs for Promoting Science and Technology, Grant-in-Aids for Scientific Research, R&D for Next Generation IT by MEXT, Hitachi Kurata-Memorial Science & Technology Foundation, and PRESTO JST. One of the authors (H.T.L.) acknowledges T. S. Chin for valuable discussions, and the financial support from the government of the Republic of China.

[1] H. Munekata, H. Ohno, S. von Molnar, A. Segmuller, L. L. Chang, and L. Esaki, Phys. Rev. Lett. **63**, 1849 (1989); H. Munekata, H. Ohno, R. R. Ruf, R. J. Gambino, and L. L. Chang, J. Cryst. Growth **111**, 1011 (1991).

[2] H. Ohno, H. Munekata, T. Penney, S. von Molnar, and L. L. Chang, Phys. Rev. Lett. **68**, 2664 (1992).

[3] H. Ohno, A. Shen, F. Matsukura, A. Oiwa, A. Endo, S. Katsumoto, and Y. Iye, Appl. Phys. Lett. **69**, 363 (1996).

[4] T. Hayashi, M. Tanaka, T. Nishinaga, H. Shimada, H. Tsuchiya, and Y. Ootuka, J. Cryst. Growth **175/176**, 1063 (1997).

[5] T. Schallenberg and H. Munekata, Appl. Phys. Lett. **89**, 042507 (2006).

[6] T. Jungwirth, K. Y. Wang, J. Mašek, K. W. Edmonds, Jürgen König, Jairo Sinova, M. Polini, N. A. Goncharuk, A. H. MacDonald, M. Sawicki, A. W. Rushforth, R. P. Campion, L. X. Zhao, C. T. Foxon, and B. L. Gallagher, Phys. Rev. B **72**, 165204 (2005); S. Ohya, K. Ohno, and M. Tanaka, Appl. Phys. Lett. **90**, 112503 (2007).

[7] S. Ohya, H. Kobayashi, and M. Tanaka, Appl. Phys. Lett. **83**, 2175 (2003).

[8] Ahsan M. Nazmul, S. Sugahara, and M. Tanaka, Appl. Phys. Lett. **80**, 3120 (2002).

[9] A. M. Nazmul, S. Sugahara, and M. Tanaka, Phys. Rev. B **67**, 241308(R) (2003).

[10] A. M. Nazmul, T. Amemiya, Y. Shuto, S. Sugahara, and M. Tanaka, Phys. Rev. Lett. **95**, 017201 (2005).

[11] H. X. Tang, R. K. Kawakami, D. D. Awschalom, and M. L. Roukes, Phys. Rev. Lett. **90**, 107201 (2003).

[12] U. Welp, V. K. Vlasko-Vlasov, X. Liu, J. K. Furdyna, and T. Wojtowicz, Phys. Rev. Lett. **90**, 167206 (2003).

[13] M. Sawicki, K.-Y. Wang, K. W. Edmonds, R. P. Campion, C. R. Staddon, N. R. S. Farley, C. T. Foxon, E. Papis, E. Kaminska, A. Piotrowska, T. Dietl, and B. L. Gallagher, Phys. Rev. B **71**, 121302(R) (2005).

[14] K. Y. Wang, K. W. Edmonds, R. P. Campion, L. X. Zhao, C. T. Foxon, and B. L. Gallagher, Phys. Rev. B **72**, 085201 (2005).

[15] T. C. Kreutz, W. D. Allen, E. G. Gwinn, D. D. Awschalom, and A. C. Gossard, Phys. Rev. B **69**, 081302(R) (2004).

[16] U. Welp, V. K. Vlasko-Vlasov, A. Menzel, H. D. You, X. Liu, J. K. Furdyna, and T. Wojtowicz, Appl. Phys. Lett. **85**, 260 (2004).

[17] K. Hamaya, T. Taniyama, Y. Kitamoto, R. Moriya, and H. Munekata, J. Appl. Phys. **94**, 7657 (2003).

[18] K. Hamaya, T. Taniyama, Y. Kitamoto, T. Fujii, and Y. Yamazaki, Phys. Rev. Lett. **94**, 147203 (2005).

[19] Jan H. Fluitman, J. Appl. Phys. **52**, 2468 (1981).

[20] D. Y. Kim, B. S. Park, and C. G. Kim, J. Appl. Phys. **88**, 3490 (2000).

[21] S. Nakagawa, I. Sasaki, and M. Naoe, J. Appl. Phys. **91**, 8354 (2002).

[22] Sarbanoo Das, Hironori Yoshikawa, and Shigeki Nakagawa, J. Appl. Phys. **93**, 8098 (2003).

[23] S. T. B. Goennenwein, S. Russo, A. F. Morpurgo, T. M. Klapwijk, W. Van Roy, and J. DeBoeck, Phys. Rev. B **71**, 193306 (2005).

[24] Y. Bason, L. Klein, J. B. Yau, X. Hong, and C. H. Ahn, Appl. Phys. Lett. **84**, 2593 (2004).

[25] R. P. Cowburn, S. J. Gray, J. Ferre, J. A. C. Bland, and J. Miltat, J. Appl. Phys. **78**, 7210 (1995).

[26] X. Liu, Y. Sasaki, and J. K. Furdyna, Phys. Rev. B **67**, 205204 (2003).

[27] T. Dietl, H. Ohno, and F. Matsukura, Phys. Rev. B **63**, 195205 (2001).
[28] S. C. Masmanidis, H. X. Tang, E. B. Myers, M. Li, K. De Greve, G. Vermeulen, W. V. Roy, and M. L. Roukes, Phys. Rev. Lett. **95**, 187206 (2005).
[29] J. Fernández-Rossier and L. J. Sham, Phys. Rev. B **64**, 235323 (2001).
[30] J. J. Krebs, B. T. Jonkers, and G. A. Prinz, J. Appl. Phys. **61**, 2596 (1987); E. M. Kneedler, B. T. Jonker, P. M. Thibado, R. J. Wagner, B. V. Shanabrook, and L. J. Whitman, Phys. Rev. B **56**, 8163 (1997).
[31] Y. B. Xu, D. J. Freeland, M. Tselepi, and J. A. C. Bland, Phys. Rev. B **62**, 1167 (2000).
[32] A. Shen, F. Matsukura, S. P. Guo, Y. Sugawara, H. Ohno, M. Tani, H. Abe, and H. C. Liu, J. Cryst. Growth **201/202**, 679 (1999).
[33] D. Kitchen, A. Richardella, Jian-Ming Tang, M. E. Flatte, and A. Yazdani, Nature (London) **442**, 436 (2006).
[34] K. Pappert, S. Humpfner, J. Wenisch, K. Brunner, C. Gould, G. Schmidt, and L. W. Molenkamp, Appl. Phys. Lett. **90**, 062109 (2007).
[35] K. Pappert, C. Gould, M. Sawicki, J. Wenisch, K. Brunner, G. Schmidt, and L. W. Molenkamp, New J. Phys. **9**, 354 (2007).